Smart Materials and Structures

PURPOSE-LED PUBLISHING™

FAST TRACK COMMUNICATION

Mechanical and functional properties of amorphous–crystalline thin ribbons of $Ti_{50}Ni_{25}Cu_{25}$ and $Ti_{40.7}Hf_{9.5}Ni_{44.8}Cu_5$ shape memory alloys

To cite this article: S Belyaev *et al* 2011 *Smart Mater. Struct.* **20** 082003

View the article online for updates and enhancements.

You may also like

- Structural and magnetocaloric properties of FeNi high entropy alloys
Kagan Sarlar, Atakan Tekgül, Nil Küçük et al.
- Microstructures and shape memory characteristics of Ti–25Ni–25Cu(at.%) alloy ribbons
Tae-hyun Nam, Soo-moon Park, Tae-yeon Kim et al.
- Study of nanoindentation behavior of NiCrCoAl medium entropy alloys under indentation process using molecular dynamics
Thi-Thuy Binh Ngo, Van-Thuc Nguyen and Te-Hua Fang

This content was downloaded from IP address 132.230.196.78 on 04/11/2026 at 15:51

Smart Mater. Struct. **20** (2011) 082003 (6pp) doi:10.1088/0964-1726/20/8/082003

FAST TRACK COMMUNICATION

Mechanical and functional properties of amorphous–crystalline thin ribbons of $Ti_{50}Ni_{25}Cu_{25}$ and $Ti_{40.7}Hf_{9.5}Ni_{44.8}Cu_5$ shape memory alloys

S Belyaev, N Resnina and V Slesarenko

Faculty of Mathematics and Mechanics, Saint Petersburg State University, Universitetskii Prospekt, 28, Saint Petersburg, 198504, Russia

E-mail: sl.slesarenko@gmail.com

Received 10 May 2011, in final form 30 June 2011
Published 28 July 2011
Online at stacks.iop.org/SMS/20/082003

Abstract

Amorphous melt spun ribbons of $Ti_{50}Ni_{25}Cu_{25}$ and $Ti_{40.7}Hf_{9.5}Ni_{44.8}Cu_5$ alloys were partially crystallized to different volume fractions of the crystalline phase from 0 to 100%. The mechanical and functional properties of amorphous–crystalline thin ribbons were studied. It was shown that the fully amorphous sample of $Ti_{50}Ni_{25}Cu_{25}$ alloy was deformed elastically up to 2.2% and then it was deformed plastically up to breaking. The fully amorphous sample of $Ti_{40.7}Hf_{9.5}Ni_{44.8}Cu_5$ alloy was deformed elastically up to failure and plastic deformation was not observed. It was found that amorphous–crystalline samples demonstrated the shape memory effect on heating. The maximum recovered strain was 3.3% in fully crystallized $Ti_{50}Ni_{25}Cu_{25}$ alloy and it attained 5% in $Ti_{40.7}Hf_{9.5}Ni_{44.8}Cu_5$ alloy. The $Ti_{40.7}Hf_{9.5}Ni_{44.8}Cu_5$ alloy demonstrated the two-way shape memory effect if the amorphous and crystalline phases co-existed in the sample.

1. Introduction

The tendency towards reduction of the dimensions of conventional devices makes the development of micro-electro-mechanical systems (MEMS) very attractive for scientists and engineers. MEMS usually consist of a microprocessor, microsensor and/or microactuator. The main aim of the microsensor is to receive data on the variation in some physical properties (pressure, speed, acceleration, etc). The basic goal of the microactuator is the performance of an action (movement). In this case, the materials for microactuators must be able to be displaced and to generate some forces. From this point of view, the shape memory alloys (SMA) are good candidates for the active elements of microactuators due to their ability to recover from large inelastic strain (up to 10%) and for having high recovery stress (up to 1000 MPa) [1–4]. The small dimensions of MEMS impose requirements on the sizes of SMA elements, which must not exceed hundreds of micrometers. One way to fabricate SMA thin ribbons is rapid solidification. This allows one to produce ribbons with a thickness of tens of micrometers. The peculiarity of this method is that the structure of the melt spun ribbons may be amorphous. At the same time only the crystalline samples demonstrate the shape memory effects; thus, annealing the melt spun thin ribbon is necessary for crystallization of the alloys. Crystallization may be carried out in two ways—by heating the sample up to a temperature which is higher than the crystallization temperature (dynamic crystallization) or by isothermal holding of the sample at a temperature which is lower than the crystallization temperature (isothermal crystallization). The parameters of the crystalline structure, such as grain size and precipitates, are controlled by the parameters of the crystallization process such as heating rate for dynamic crystallization and temperature and duration of isothermal crystallization [5–8]. At the same time, the crystallization process may be interrupted before

 © 2011 IOP Publishing Ltd Printed in the UK & the USA

completion. In such cases, the structure of the alloy becomes amorphous–crystalline. The properties of such partially crystallized SMAs depend on grain size and the ratio between the amorphous and the crystalline volume fractions [9–12].

In [12] it was found that all the characteristics of the martensitic transformation in amorphous–crystalline Ti–Hf–Ni–Cu and Ti–Ni–Cu thin ribbons depended on the fraction of the crystalline phase. The temperatures of both direct and reverse transitions increased as the volume fraction of the crystalline phase grew. The temperature range of the transformation and its hysteresis decreased as the amount of the crystalline phase increased. Moreover it was observed that the martensitic transformation from the cubic B2 phase to the monoclinic B19′ phase occurring in Ti–Hf–Ni–Cu alloys was more sensitive to the structure of the alloy than a transition from the cubic B2 to the orthorhombic B19 phase occurring in $Ti_{50}Ni_{25}Cu_{25}$ [13]. This was due to the difference in the crystallographic shear strain due to the martensitic transformation [14]. As shape memory effects are determined by the martensitic transformation characteristics, one may assume that the functional properties of amorphous–crystalline TiNi-based thin ribbons must depend on the fraction of the crystalline phase too. Moreover an additional effect may be caused by co-existence of the amorphous and the crystalline phases, since the interface between them may be the place for preferable formation of martensite crystals which may result in the formation of stresses [9]. The aim of this work is to study the influence of the crystalline phase fraction on the mechanical properties and shape memory effects in amorphous–crystalline thin ribbons of $Ti_{40.7}Hf_{9.5}Ni_{44.8}Cu_5$ and $Ti_{50}Ni_{25}Cu_{25}$ alloys.

2. Experimental procedure

Amorphous thin ribbons (40 μm in thickness) of $Ti_{40.7}Hf_{9.5}Ni_{44.8}Cu_5$ and $Ti_{50}Ni_{25}Cu_{25}$ alloys were obtained by rapid solidification of the melt. X-ray analysis revealed the fully amorphous state of the ribbons. Thin amorphous samples of dimensions 5 mm × 2 mm × 0.04 mm of $Ti_{50}Ni_{25}Cu_{25}$ and $Ti_{40.7}Hf_{9.5}Ni_{44.8}Cu_5$ alloys were subjected to partial crystallization at temperatures of 420 and 470 °C, according to the method described in [12]. The samples were kept in the differential scanning calorimetry (DSC) apparatus at a constant crystallization temperature for a time which was less then the time of the complete crystallization. The crystallization was interrupted by rapidly quenching the samples in air and the heat of partial crystallization $H_{\mathrm{p.c.}}$ was estimated. After such a procedure, the samples were in two phase stages—crystalline and amorphous. The value of the crystalline volume fracture (Φ) was estimated as the ratio of the heat of the partial crystallization to the heat of complete crystallization for each sample. For more detail on sample preparation, see [12]. The method of controlling the partial crystallization allows the samples of $Ti_{50}Ni_{25}Cu_{25}$ alloy to be obtained with 0%, 50%, 70% and 100% volume fraction of the crystalline phase (Φ) and the samples of $Ti_{40.7}Hf_{9.5}Ni_{44.8}Cu_5$ alloy with Φ = 0%, 40%, 70% and 100%. The crystal structure of amorphous–crystalline samples was studied by x-ray analysis with Cu Kα radiation at different temperatures. The martensitic transformation in the samples was studied by the DSC method on cooling from 100 to −120 °C and on heating up to 100 °C with a cooling/heating rate of 10 °C min^{-1}. The temperatures of the martensitic transformation were determined according to the ASTM standard test method F 2004-00.

The mechanical and functional properties of the amorphous–crystalline samples were studied using the following method. Samples were deformed up to some strain at the temperature at which the crystalline phase was in the martensite state (see figure 1(a)), and then unloaded (see figure 1(b)). After that, samples were heated up to the temperature at which the crystalline phase was in the austenite state (see figure 1(c)) and then cooled down to the initial temperature (see figure 1(d)). The samples were then deformed to the greater strain and the described procedure was repeated. At each step the samples were photographed and their profiles were digitized (see figure 2) to determine the radius of bending (R) and measure the strain of the samples. The strain was measured in the outer fiber of the stripe sample as $\varepsilon = \frac{h}{2R} \times 100\%$, where the h is the thickness of the stripe (40 μm) and the R is the bending radius.

The given strain (ε) was measured as the strain at the first step after loading, the residual strain (ε_{r}) was equal to the strain at the second step after unloading. The value of the shape memory effect ($\varepsilon^{\mathrm{sm}}$) was determined as the difference between the strains at the second (after unloading) and third (after heating) steps, and the value of the two-way shape memory effect ($\varepsilon^{\mathrm{twsm}}$) was determined as the difference between strain at the fourth (after cooling) and the third (after heating) steps. This procedure allowed us to study the influence of the given strain on the residual strain, and the dependence of the values of shape memory and two-way shape memory effects on residual strain.

3. Results and discussion

Figure 3 shows the x-ray patterns of the fully crystallized thin ribbons of $Ti_{50}Ni_{25}Cu_{25}$ (see figure 3(a)) and $Ti_{40.7}Hf_{9.5}Ni_{44.8}Cu_5$ (see figure 3(b)) alloys in austenite and martensite states. It can be seen that in the fully crystallized state both alloys have the austenite B2-type structure at a high temperature, but at low temperature these alloys have different structures of the martensite phase. The $Ti_{50}Ni_{25}Cu_{25}$ alloy is in the orthorhombic B19 phase, and the $Ti_{40.7}Hf_{9.5}Ni_{44.8}Cu_5$ is in the monoclinic B19′ phase. Hence the crystalline phase in $Ti_{50}Ni_{25}Cu_{25}$ alloy undergoes the B2 ↔ B19 transition and in the $Ti_{40.7}Hf_{9.5}Ni_{44.8}Cu_5$ alloy B2 ↔ B19′ transformation occurs. This is verified by the DSC data. The temperatures and heat of the martensitic transformations are given in tables 1 and 2. It can be seen that an increase in volume fraction of the crystalline phase results in a rise in transformation temperatures and enthalpy, which is in good agreement with previous studies [12]. It is very important to note that the amorphous–crystalline $Ti_{40.7}Hf_{9.5}Ni_{44.8}Cu_5$ alloy demonstrates unusual kinetics of the martensitic transformation, as the direct transformations take place in a narrow temperature range and

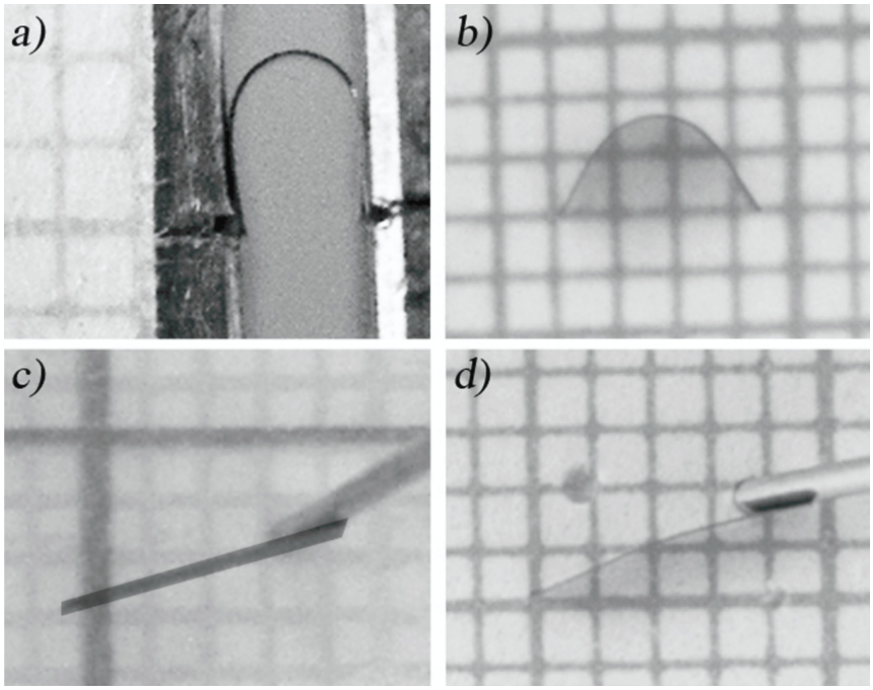


Figure 1. Photos of the sample after loading (a), after unloading (b), after heating (c), and after cooling (d).

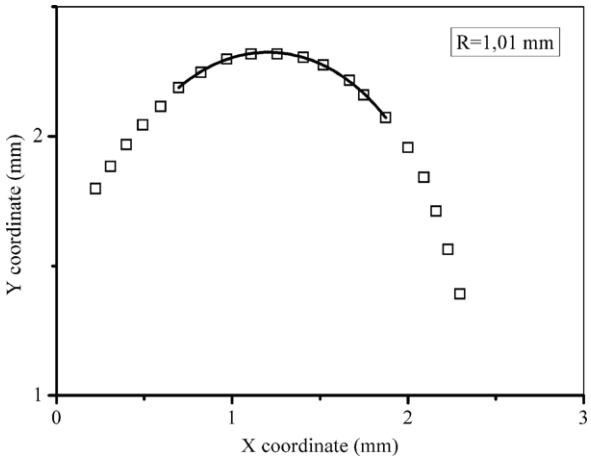


Figure 2. An example of digitizing the sample profile.

Table 1. Temperatures of martensitic transformations in samples of $Ti_{50}Ni_{25}Cu_{25}$ alloy with different volume fractions of the crystalline phase.

Φ (%)	M_s (C)	M_f (C)	A_s (C)	A_f (C)	E (J g^{-1})
50	62	58	61	70	8.77
70	63	60	65	71	13.08
100	67	64	67	72	15.1

the reverse transitions occur in a wide temperature range; also, the value of hysteresis is very large.

Figure 4(a) shows the dependence of residual strain (ε_r) on given strain (ε), obtained at deformation of the samples of $Ti_{50}Ni_{25}Cu_{25}$ alloy with different volume fractions of the crystalline phase at a temperature of 25 °C. There are two stages on the ε_r versus ε curve measured in the fully amorphous sample.

Table 2. Temperatures of martensitic transformations in samples of $Ti_{40.7}Hf_{9.5}Ni_{44.8}Cu_5$ alloy with different volume fractions of the crystalline phase.

Φ (%)	M_s (C)	M_f (C)	A_s (C)	A_f (C)	E (J g^{-1})
40	−56	−69	−17	12	2.4
70	−27	−32	2	43	7
100	−5	−8	32	52	18.7

In the case of $\varepsilon < 2.2\%$ the strain recovers completely on unloading and ε_r is equal to zero. Otherwise, at $\varepsilon > 2.2\%$ the residual strain (ε_r) is observed after unloading. Hence the amorphous sample deforms elastically when the given strain is less than 2.2%, and it deforms plastically when the given strain exceeds 2.2%. If any crystalline phase exists in the alloy, then deformation of the samples by even a small strain results in the appearance of residual strain. This is due to the crystalline phase at a temperature of 25 °C being in the martensite state and crystalline volumes are deformed by the martensite reorientation mechanism. An increase in volume fraction of the crystalline phase leads to an increase in residual strain. For example, a fully amorphous sample deformed by up to 3% exhibits a residual strain equal to 0.75%, similarly a sample at 70% of the crystalline phase demonstrates $\varepsilon_r \approx$ 1.4%, and finally in a fully crystalline sample 2% of residual strain is observed.

Figure 4(b) shows the dependences of the value of the shape memory effect (ε^{sm}) on residual strain (ε_r) obtained in amorphous–crystalline samples of $Ti_{50}Ni_{25}Cu_{25}$ alloy. One may observe that the value of the shape memory effect increases linearly up to some strain (ε_{cr}) and slightly changes

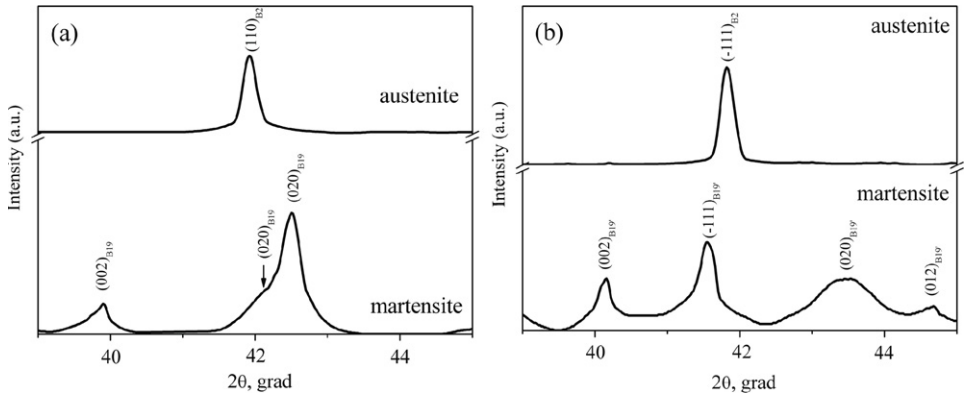


Figure 3. X-ray patterns obtained in austenite and martensite states of $Ti_{50}Ni_{25}Cu_{25}$ (a) and $Ti_{40.7}Hf_{9.5}Ni_{44.8}Cu_5$ (b) alloys.

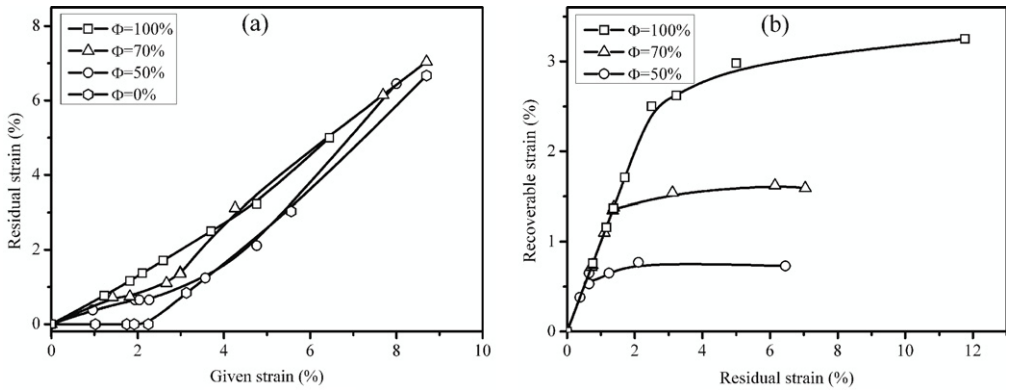


Figure 4. Residual strain versus given strain (a) and recoverable strain versus residual strain (b) curves obtained in amorphous–crystalline samples of $Ti_{50}Ni_{25}Cu_{25}$ alloy with different volume fractions of the crystalline phase. The deformation temperature is 25°C.

further. The value of ε_{cr} depends on the volume fraction of the crystalline phase (Φ). It is found that the maximum of recovered strain is equal to 3.3% in the fully crystalline sample. The ability of the alloy to recover from strain is usually estimated by the strain recovery coefficient (K). This value is calculated from the ratio of the value of the shape memory effect to the residual strain. Figure 5 shows a variation in the strain recovery coefficient on residual strain for $Ti_{50}Ni_{25}Cu_{25}$ samples with different volume fractions of the crystalline phase. In the first stage when $\varepsilon_r < \varepsilon_{cr}$ the value of K is equal to 100%. In other words, inelastic strain recovers totally on heating.

Apparently, at such a level of strain the alloy is only deformed by the martensite reorientation mechanism. In the case of $\varepsilon_r > \varepsilon_{cr}$, the value of K decreases significantly and irreversible strain accumulates in the sample. An increase in volume fraction of the crystalline phase leads to an increase in the interval of the first stage because a larger volume of alloy can be deformed by martensite reorientation. The range of the first stage in the fully crystallized sample is about 2.5–3%. No strain variation is observed on cooling and heating of the deformed amorphous–crystalline samples. This means that the amorphous–crystalline $Ti_{50}Ni_{25}Cu_{25}$ alloy does not demonstrate a two-way shape memory effect.

Figure 6 shows dependences of residual strain (ε_r) on given strain (ε), obtained for deformation of $Ti_{40.7}Hf_{9.5}Ni_{44.8}Cu_5$ alloy with different volume fractions of the crystalline phase at a temperature of −196 °C (a) and dependences of the value of the shape memory effect on residual strain (b). One may see that the mechanical behavior of the amorphous–crystalline samples of $Ti_{40.7}Hf_{9.5}Ni_{44.8}Cu_5$ alloy is similar to the behavior demonstrated by the samples of $Ti_{50}Ni_{25}Cu_{25}$

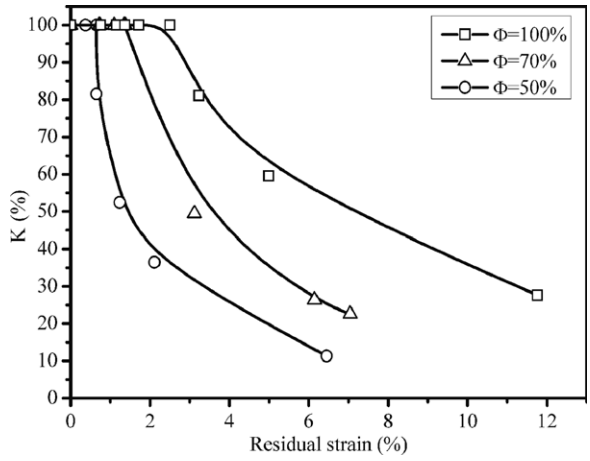


Figure 5. Strain recovery coefficient versus residual strain curves, obtained in samples of $Ti_{50}Ni_{25}Cu_{25}$ alloy with different volume fractions of the crystalline phase.

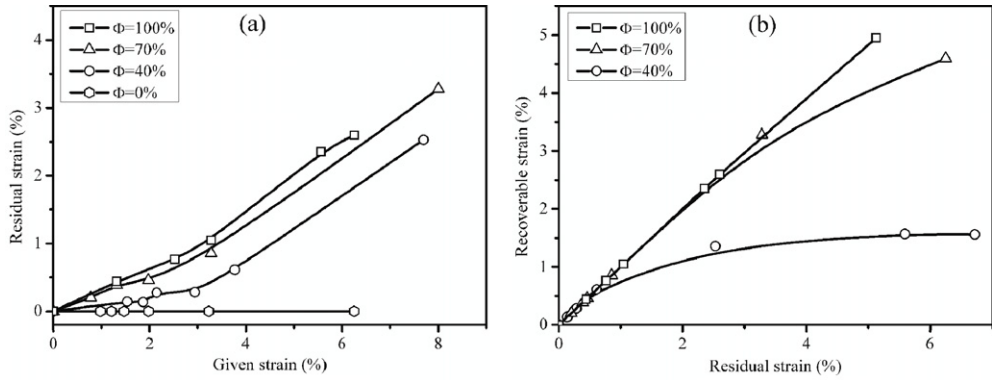


Figure 6. Residual strain versus given strain (a) and recoverable strain versus residual strain (b) curves obtained in amorphous–crystalline samples of $Ti_{40.7}Hf_{9.5}Ni_{44.8}Cu_5$ alloy with different volume fractions of the crystalline phase.

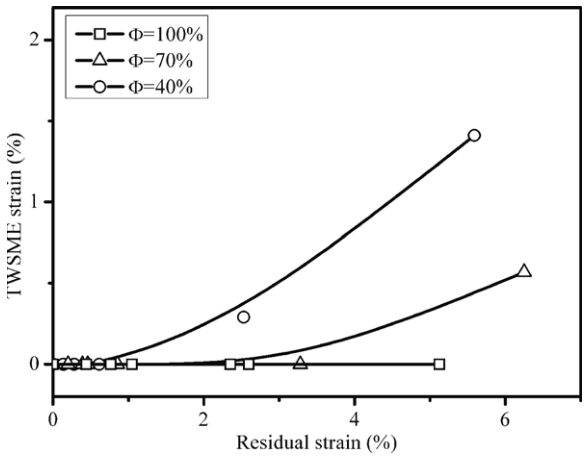


Figure 7. Dependences of value of the two-way shape memory effect (TWSME) on residual strain obtained in samples of $Ti_{40.7}Hf_{9.5}Ni_{44.8}Cu_5$ alloy with different volume fractions of the crystalline phase.

alloy (see figure 4(a)). However, attention should be paid to the fact that the amorphous sample $Ti_{40.7}Hf_{9.5}Ni_{44.8}Cu_5$ alloy deforms fully elastically by up to 6% before failure (see figure 6(a)). Moreover, the value of the shape memory effect (see figure 6(b)) is about two times higher than in the $Ti_{50}Ni_{25}Cu_{25}$ alloy (see figure 4(b)). So in the fully crystallized $Ti_{40.7}Hf_{9.5}Ni_{44.8}Cu_5$ sample the maximum recoverable strain $\varepsilon_{cr} = 5\%$. This is due to the B2 $\rightarrow$ B19′ transformation being accompanied by a larger shear strain than the B2 $\rightarrow$ B19 transition [14].

Contrary to the $Ti_{50}Ni_{25}Cu_{25}$ alloy, where no two-way shape memory effect is observed, the $Ti_{40.7}Hf_{9.5}Ni_{44.8}Cu_5$ samples with volume fractions of the crystalline phase of 40% and 70% demonstrate a good two-way shape memory effect (see figure 7). It is essential to note that the two-way shape memory effect is not found in fully crystallized $Ti_{40.7}Hf_{9.5}Ni_{44.8}Cu_5$ samples. Thus the co-existence of amorphous and crystalline phases is a required condition for the two-way shape memory effect. Probably during the deformation of the amorphous–crystalline sample the internal stresses appear on the amorphous/crystalline interface. Additionally, according to [9], the interfaces between the amorphous and crystalline phases form the site for the nucleation of martensite variants. In this case the existence of oriented internal stresses on the interface must result in the nucleation of martensite variants where the crystallographic shift coincides with the direction of internal stresses. As a result, a variation in macroscopic strain is observed in the sample. The higher the deformation of the amorphous–crystalline sample, the higher the internal stresses formed on the amorphous/crystalline interface and the higher the value of the two-way shape memory effect. The shear strain of B2 $\rightarrow$ B19 transformation is less than the shear strain of B2 $\rightarrow$ B19′ transformation. As a result, the internal stresses appearing in $Ti_{50}Ni_{25}Cu_{25}$ alloy are less then in $Ti_{40.7}Hf_{9.5}Ni_{44.8}Cu_5$ alloy. That may be the reason why a two-way shape memory effect is not observed in $Ti_{50}Ni_{25}Cu_{25}$ alloy.

Thus the results of the study have shown that the amorphous–crystalline samples demonstrate good shape memory effects. It was found that the value of the shape memory effect in $Ti_{40.7}Hf_{9.5}Ni_{44.8}Cu_5$ alloy is two times higher than that in $Ti_{50}Ni_{25}Cu_{25}$. Moreover, a two-way shape memory effect is found in the amorphous–crystalline $Ti_{40.7}Hf_{9.5}Ni_{44.8}Cu_5$ alloy.

4. Summary

Summarizing the data obtained one may conclude:

(1) The amorphous $Ti_{50}Ni_{25}Cu_{25}$ alloy deforms elastically up to 2.2%, than plastic deformation is observed. The amorphous $Ti_{40.7}Hf_{9.5}Ni_{44.8}Cu_5$ alloy deforms elastically up to failure.

(2) The amorphous–crystalline samples demonstrate the shape memory effect. Increase in the volume fraction of the crystalline phase results in a rise of the recoverable strain. It was found that the recoverable strain observed in the $Ti_{40.7}Hf_{9.5}Ni_{44.8}Cu_5$ alloy was twice as high as in the $Ti_{50}Ni_{25}Cu_{25}$ alloy. This was due to the different type of martensitic transformation occurring in these alloys. The $Ti_{40.7}Hf_{9.5}Ni_{44.8}Cu_5$ alloy underwent the B2 $\leftrightarrow$ B19′ transformation accompanied by a larger shear strain than the B2 $\leftrightarrow$ B19 transitions occurring in the $Ti_{50}Ni_{25}Cu_{25}$ alloy.

(3) The $Ti_{40.7}Hf_{9.5}Ni_{44.8}Cu_5$ alloys with volume fractions of the crystalline phase of 40% and 70% demonstrate a good two-way shape memory effect. Apparently the existence of the interfaces between the amorphous and crystalline phases are the preferable sites for the creation of the oriented internal stresses, which are responsible for the observation of two-way shape memory effect.

Acknowledgment

The authors are grateful to Dr A Shelyakov for preparation of the amorphous thin ribbons.

References

[1] Lucaci M, Orban R L, Tsakiris V and Cirska D 2008 Shape memory alloys for MEMS components made by powder metallurgy processes *Proc. 2008 2nd Electronics System-Integration Technology Conf.* pp 1241–2

[2] Namazu T, Hashizume A and Inoue S 2007 Thermomechanical tensile characterization of Ti–Ni shape memory alloy films for design of MEMS actuator *Sensors Actuators* A **139** 178–86

[3] Fu Y, Du H, Huang W, Zhang S and Hu M 2004 TiNi-based thin films in MEMS applications: a review *Sensors Actuators* A **112** 395–408

[4] Namazu T, Tashiro Y and Inoue S 2007 Ti–Ni shape memory alloy film-actuated microstructures for a MEMS probe card *J. Micromech. Microeng.* **17** 154–62

[5] Motemani Y, Tan M J, White T J and Banas A 2011 Evolution of structural, surficial and mechanical properties of titanium–nickel–copper thin films during rapid thermal annealing *Surf. Coat. Technol.* **205** 3147–57

[6] Li Y, Meng F, Wang J and Wang Y 2004 The characterization of crystalline particle growth in TiNi thin films *J. Appl. Crystallogr.* **37** 1007–9

[7] Matsuda M, Shimada Y, Murasaki T, Nishida M, Ishikawa K and Aoki K 2009 Crystallization and microstructure changes in rapidly solidified $Nb_{20}Ti_{40}Ni_{40}$ hydrogen permeation alloy *J. Alloys Compounds* **485** 773–7

[8] Liu Y S, Xu D, Jiang B H, Yuan Z Y and Houtte P 2005 The effect of crystallization procedure on microstructure and characteristics of sputter-deposited TiNi shape memory thin films *J. Micromech. Microeng.* **15** 575–9

[9] Waitz T and Karnthaler H P 2004 Martensitic transformation of NiTi nanocrystals embedded in an amorphous matrix *Acta Mater.* **52** 5461–9

[10] Nakayama H, Tsuchiya K and Umemoto M 2001 Crystal refinement and amorphisation by cold polling in TiNi shape memory alloys *Scr. Mater.* **44** 1781–5

[11] Santamarta R and Schryvers D 2004 Effect of amorphous–crystalline interfaces on the martensitic transformation in $Ti_{50}Ni_{25}Cu_{25}$ *Scr. Mater.* **50** 1423–7

[12] Resnina N, Belyaev S and Shelyakov A 2008 Martensitic transformation in amorphous–crystalline Ti–Ni–Cu and Ti–Hf–Ni–Cu thin ribbons *Eur. Phys. J.* **158** 21–6 (Special topics)

[13] Resnina N, Belyaev S and Shelyakov A 2009 Influence of the dynamic crystallization conditions on the martensitic transformation in the $Ti_{40.7}Hf_{9.5}Ni_{39.8}Cu_{10}$ shape memory alloy *Z. Metallkd.* **100** 356–8
Resnina N, Belyaev S and Shelyakov A 2009 Influence of the dynamic crystallization conditions on the martensitic transformation in the $Ti_{40.7}Hf_{9.5}Ni_{39.8}Cu_{10}$ shape memory alloy *Int. J. Mater. Res.* **100** 356–8 (Engl. transl.)

[14] Otsuka K and Ren X 2005 Physical metallurgy of Ti–Ni based shape memory alloys *Prog. Mater. Sci.* **50** 511–678